Journal of Physics D: Applied Physics

PAPER • OPEN ACCESS

Towards smooth (010) β-Ga_2O_3 films homoepitaxially grown by plasma assisted molecular beam epitaxy: the impact of substrate offcut and metal-to-oxygen flux ratio

To cite this article: P Mazzolini and O Bierwagen 2020 *J. Phys. D: Appl. Phys.* **53** 354003

View the article online for updates and enhancements.

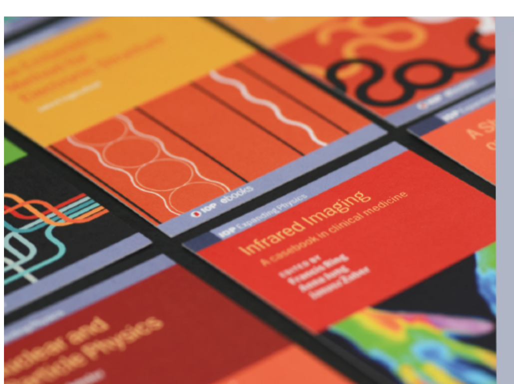
IOP ebooks™

Bringing together innovative digital publishing with leading authors from the global scientific community.

Start exploring the collection–download the first chapter of every title for free.

This content was downloaded from IP address 160.78.34.119 on 18/09/2020 at 10:20

OPEN ACCESS
IOP Publishing

Journal of Physics D: Applied Physics

J. Phys. D: Appl. Phys. **53** (2020) 354003 (9pp)

https://doi.org/10.1088/1361-6463/ab8eda

Towards smooth (010) β-Ga_2O_3 films homoepitaxially grown by plasma assisted molecular beam epitaxy: the impact of substrate offcut and metal-to-oxygen flux ratio

P Mazzolini and O Bierwagen

Paul-Drude-Institut für Festkörperelektronik, Leibniz-Institut im Forschungsverbund Berlin e.V., Hausvogteiplatz 5–7, Berlin, 10117 Germany

E-mail: mazzolini@pdi-berlin.de and bierwagen@pdi-berlin.de

Received 10 March 2020, revised 23 April 2020
Accepted for publication 30 April 2020
Published 15 June 2020

Abstract

Smooth interfaces and surfaces are beneficial for most (opto)electronic devices that are based on thin films and their heterostructures. For example, smoother interfaces in (010) β-Ga_2O_3/$(Al_xGa_{1-x})_2O_3$ heterostructures, whose roughness is ruled by that of the β-Ga_2O_3 layer, can enable higher mobility 2-dimensional electron gases by reducing interface roughness scattering. To this end we experimentally prove that a substrate offcut along the [001] direction allows to obtain smooth β-Ga_2O_3 layers in (010)-homoepitaxy under metal-rich deposition conditions. Applying In-mediated metal-exchange catalysis (MEXCAT) in molecular beam epitaxy at high substrate temperatures ($T_g = 900\ °C$) we compare the morphology of layers grown on (010)-oriented substrates having different unintentional offcuts. The layer roughness is generally ruled by (i) the presence of (110)- and $(\bar{1}10)$-facets visible as elongated features along the [001] direction (rms < 0.5 nm), and (ii) the presence of trenches (5–10 nm deep) orthogonal to [001]. We show that an unintentional substrate offcut of only $\approx 0.1°$ almost oriented along the [001] direction suppresses these trenches resulting in a smooth morphology with a roughness exclusively determined by the facets, i.e. rms $\approx$ 0.2 nm. Since we found the facet-and-trench morphology in layer grown by MBE with and without MEXCAT, we propose that the general growth mechanism for (010)-homoepitaxy is ruled by island growth whose coalescence results in the formation of the trenches. The presence of a substrate offcut in the [001] direction can allow for step-flow growth or island nucleation at the step edges, which prevents the formation of trenches. Moreover, we give experimental evidence for a decreasing surface diffusion length or increasing nucleation density on the substrate surface with decreasing metal-to-oxygen flux ratio. Based on our experimental results we can rule-out step bunching as cause of the trench formation as well as a surfactant-effect of indium during MEXCAT.

Keywords: Ga_2O_3, molecular beam epitaxy, homoepitaxy, monolayer steps, surface diffusion length, catalysis, semiconducting oxides

(Some figures may appear in colour only in the online journal)

Original content from this work may be used under the terms of the Creative Commons Attribution 4.0 licence. Any further distribution of this work must maintain attribution to the author(s) and the title of the work, journal citation and DOI.

1. Introduction

Gallium oxide in its most thermodynamically stable monoclinic structure (space group C2 m^{-1}, a = 12.214 Å, b = 3.0371 Å, c = 5.8981 Å, β = 103.83°) [1] β-Ga_2O_3 has recently been proposed as a promising material for power electronics [2]. The possibility to deposit it on native substrates grown from the melt [3] can allow for the synthesis of high quality thin films. Nonetheless, the growth of β-Ga_2O_3 is orientation-dependent, and this can affect both the structural quality [4, 5] and the growth rate [5, 6] of the deposited layers (e.g. structural defects and low deposition rate in (100)-oriented layers). For these reasons, the most widely employed substrate orientation for β-Ga_2O_3 homoepitaxy has been so far the (010) one as it prevents formation of twin defects and provides a comparably high growth rate in molecular beam epitaxy (MBE). MBE and metal-organic vapor phase epitaxy (MOVPE) are the deposition techniques that provided high quality homoepitaxial β-Ga_2O_3 layers, also enabling for a fine control of their electrical properties throughout n-type extrinsic doping [7–9], as well as the growth of modulation-doped heterostructures [10–12]. Nonetheless, different synthesis conditions can affect the electrical properties of the deposited layers through the formation of deep level acceptors that could work as electron traps in β-Ga_2O_3 (e.g. Ga-vacancies), potentially limiting both charge carrier density and mobility [13, 14]. Therefore, Ga-rich deposition conditions [13] and high growth temperatures T_g [15] have been theoretically predicted to be favorable for the synthesis of β-Ga_2O_3 layers. Unfortunately, due to the strong desorption of the intermediately formed volatile suboxide Ga_2O from the growth surface [16], the deposition of Ga_2O_3 under these conditions is challenging even in the case of (010) homoepitaxy [17]. The employment of an additional In-flux as a catalyst during Ga_2O_3 deposition in MBE, i.e. metal-exchange catalysis (MEXCAT) [18], has been shown to result in large incorporation of the impinging Ga-flux even under synthesis conditions that would not otherwise allow for layer growth (e.g. metal-rich, high T_g) with very limited In-incorporation in the deposited layer [5, 17, 18]. A similar effect has been also demonstrated using Sn as catalyzing element [19]. In particular, for β-Ga_2O_3 (010)-homoepitaxy we have shown [17] that In-mediated MEXCAT-MBE provides high quality β-Ga_2O_3 layers with almost full Ga-flux incorporation under metal-rich deposition conditions at T_g = 900 °C. Moreover, we identified that the surface roughness of the (010)-oriented layers is usually dominated by two distinct morphologies [17], both identifiable by atomic force microscopy (AFM): (i) the presence of (110) and $(\bar{1}10)$ surface equivalent facets visible as straight lines oriented along the [001] in-plane direction (highlighted in red in figure 1(a), and as pink and blue shaded planes in the atomic model of figure 1(b)), and (ii) the presence of trenches/grooves visible as irregular features running almost orthogonal to the facets (blue dotted lines in figure 1(a)). The presence of (i) facets is ruled by thermodynamics (i.e. (110) more stable surface with respect to the (010) one under reducing/metal-rich conditions), but has nonetheless been found to have a limited impact on the overall surface roughness of the deposited layers, since for high T_g it is possible to obtain peak-to-valley height of less than 0.5 nm with lateral spacing of ≈ 5–10 nm [17]. Differently, the (ii) trenches/grooves are found to be usually 5–10 nm deep with a typical trench-to-trench distance in the order of 300–500 nm [17] and could therefore be problematic for the realization of heterostructures, e.g. by reducing the mobility of 2-dimensional electron gases (2DEGs) at the interface of modulation-doped single [10–12] or double [20] β-$(Al_xGa_{1-x})_2O_3$/Ga_2O_3 structures. The formation of trenches/grooves on the surface of (010)-oriented β-Ga_2O_3 and β-$(Al_xGa_{1-x})_2O_3$ layers has been widely reported (but little commented) in literature for both MBE [7, 8, 10, 17, 21] and MOVPE [9, 22, 23].

To date, different explanations have been given for the formation of these trenches. Based on homoepitaxial growths by ozone MBE, Sasaki *et al* [8] suggested that the groove formation should be related to step-bunching along the [001] direction, given the possibility to reduce the rms of the deposited layers by lowering T_g. In contrast, smooth (010)-layers have been obtained by Okumura *et al* [7] using plasma-assisted MBE at high growth temperatures on substrates with a large 2° unintentional offcut along the [001] in-plane direction, suggesting the absence of step-bunching in favor of step-flow growth. We have recently reported a trench-free (010) β-Ga_2O_3 homoepitaxial layer deposited at T_g = 900 °C grown by In-mediated MEXCAT via plasma-assisted MBE whereas a layer deposited under the very same conditions (i.e. T_g and O-to-Ga flux ratio), but without In-mediated MEXCAT resulted in the formation of trenches, speculating on either an impact of different unintentional offcuts or an increase of the surface diffusion length due to In-mediated MEXCAT [17]. Additionally, it has been shown that In-mediated MEXCAT via plasma-assisted MBE also realized trench-free β-$(Al_xGa_{1-x})_2O_3$ layers on (010) β-Ga_2O_3 substrates [24], suggesting both a catalytic and a surfactant effect of In. A possible role of In as a surfactant has been also suggested in (100) homoepitaxy of β-$(In_xGa_{1-x})_2O_3$ via MOVPE [25].

In this work we experimentally investigate the cause of trench formation in (010) β-Ga_2O_3 homoepitaxy by plasma-assisted MBE with respect to the substrate offcut and the metal-to-oxygen flux ratio during plasma-assisted MBE.

2. Experiment

We use In-mediated MEXCAT to deposit β-Ga_2O_3 homoepitaxial layers on top of substrates with different unintentional offcuts previously measured by a combination of x-ray reflectivity (XRR) and x-ray diffraction (XRD—PANalytical X'Pert Pro MRD). The unintentionally doped substrate is electrically semiconducting due to the presence of Si impurities ($n \leq 9 \times 10^{17}$ cm^{-3}) [26]. An O-plasma treatment at T_g = 900 °C has been always performed prior to the deposition process and resulted in a featureless surface [17]. For the details regarding the experimental process and the substrate characterization please consult [17]. The offcut measurements were collected on 10 × 15 mm^2 substrates which were afterwards cut in 5 × 5 mm^2 pieces. For their in-plane orientation the skew-symmetric reflection of the (111) crystal plane was

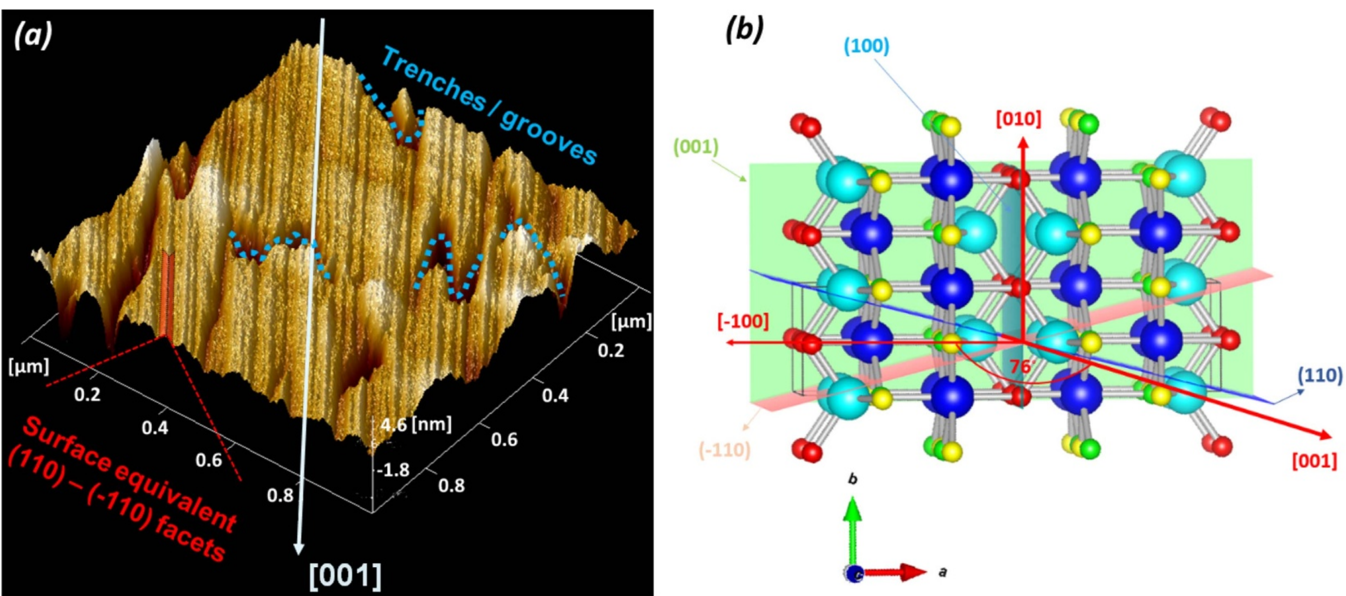

Figure 1. (a) 3-dimensional representation of an AFM image of an (010) β-Ga_2O_3 homoepitaxial layer (2d image of the same sample is reported in figure 2 (c)). The presence of two facets is exemplarily highlighted in red, while some trenches are exemplarily marked as blue dotted lines. (b) β-Ga_2O_3 atomic model with highlighted crystalline directions and lattice planes of interest. In the ball and stick model, the light and dark blue spheres are referring to the Ga(I) and Ga(II) atoms, respectively, while the yellow, green, and red ones are referring to the O(I), O(II), and O(III), respectively.

measured. We performed four different offcut measurements by rotating the in-plane direction (Φ angle) of the sample in steps of 90°, each time aligning ω for the (020) crystal planes and afterwards measuring the shift of the surface reflection with respect to this alignment ($2\theta = 0.5°$, 1/16° beam width, 0.18 mm detector slit, see figure 2(a)). The four offcut measurements were fitted with a sine function in order to determine the absolute offcut component and direction (figure 2(b)).

We found that with our experimental setup the measurement of the substrate offcut on (010) substrates can be reliably done just before the full crystal cut in 5×5 mm^2 pieces; we believe this could be related to the round edges on the sides of the (010) crystals which could induce a broadening of the surface reflection component in such a small sample size. A summary of the measured unintentional offcuts α on the four different employed substrates is reported in table 1. The expected associated terrace length has been evaluated considering monolayer steps equal to the b unit cell parameter, i.e. 0.303 nm [27]; nonetheless, consistently to what we have previously reported [17], we never identified monolayer steps before the deposition process. The film thickness was determined from XRD 'Pendellösung' fringes in the vicinity of the (020) β-Ga_2O_3 reflection in 2θ-ω scans [7, 17]. The surface morphology of the deposited layers was characterized by AFM (Bruker Dimension Edge) in the PeakForce tapping mode on two different image sizes (1x1–5x5 μm^2).

We deposited a series of samples with MEXCAT at T_g = 900 °C under identical, nominally metal-rich conditions [17] (gallium flux Φ_{Ga} = 2.2 nm^{-2} s^{-1}, indium flux Φ_{In} = 0.7 nm^{-2} s^{-1}, O-flow = 0.33 sccm—plasma power P = 300 W, growth time 30 min) on top of the four characterized substrates with different unintentional offcuts (table 1). In line with our previous report [17], under these growth conditions we were able to obtain for all the deposited layers a comparable thickness (range of 80–100 nm) without XRD-detectable In incorporation (i.e. without shift of the layer peak with respect to the (020) reflection of the substrate, e.g. red curve in figure 7(d)). The recorded thicknesses reflect a metal-incorporation between 80 and 100% with respect to the provided Φ_{Ga} [17]. Moreover, the effect of three different oxygen flows (i.e. 0.2–0.33–0.5 sccm) was investigated while maintaining constant the other deposition parameters for layers deposited on top of substrates obtained from the same Sn:Ga_2O_3 crystal (see table 1).

3. Results

Figure 3 summarizes the AFM micrographs of all the layers deposited under these conditions. They all show homogeneous morphologies as visible comparing 1x1 and 5×5 μm^2 images.

The samples deposited on substrates having the in-plane direction of their absolute offcuts 86°, 55°, and 41° away from the [001] direction (figures 3(a)–(c) respectively), all show the discussed morphological features typical of (010)-homoepitaxial layers, i.e. (110)-facets visible as straight lines oriented along the [001] direction, and several nanometer-deep irregularly shaped trenches/grooves almost orthogonally oriented to the [001] direction.

At first, we deduced the mean distance among (110)–$(\bar{1}10)$ facets from the peak-to-peak mean spacing obtained from line profiles extracted orthogonally to the [001] direction in the 1×1 μm^2 AFM images presented in figure 3 (table 2). Exemplarily, we also report in figure 4 the line profiles and the identified peaks of two β-Ga_2O_3 homoepitaxial samples deposited on substrates from two different crystals under the very same growth conditions with and without MEXCAT

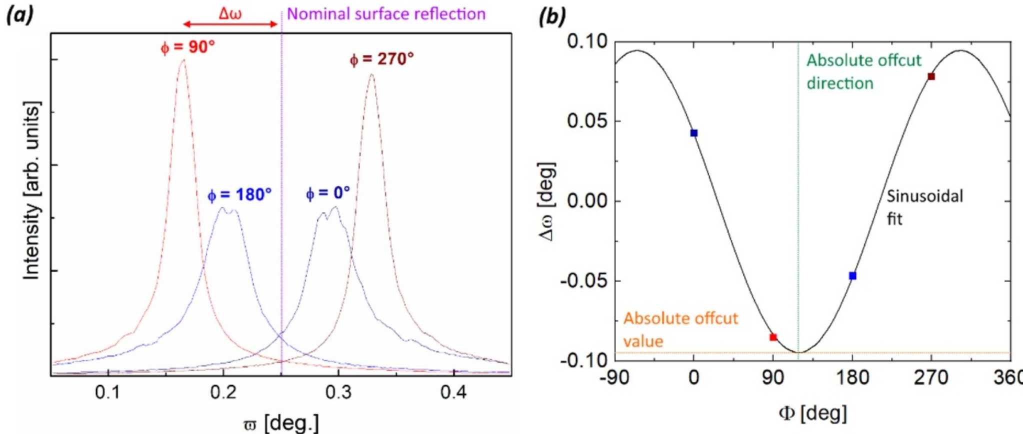

Figure 2. (a) XRD ω scans performed on the 15 × 10 mm^2 unintentionally doped Ga_2O_3 substrate (see table 1) in total reflection configuration ($2\theta = 0.5°$) in four different in-plane directions (Φ-angles) separated by 90° after ω alignment to the (020) crystal planes. For example, the $\Phi = 90°$ measurement (red curve) is performed along the [001] direction; the offcut component along that in-plane direction is reflected by the $\Delta\omega$ difference (red arrow) with respect to the nominal surface reflection ($\omega = 0.25°$, violet dotted line). (b) Sinusoidal fit of the $\Delta\omega$ offcut components evaluated in *(a)* for the same sample for the obtainment of absolute offcut value and direction (orange and green dotted line respectively).

Table 1. Measured unintentional offcuts of the (010) β-Ga_2O_3 substrates used in this study. An exemplary measurement of the unintentionally doped Ga_2O_3 substrate is reported in figure 2.

Substrate	Absolute offcut α (°)	Expected terrace length (nm)	Absolute offcut in-plane direction with respect to (001) (°)	Offcut component along [001] (°)
Fe:Ga_2O_3–1	0.12	150	86	0.01
Fe:Ga_2O_3–2	0.13	135	55	0.07
Sn:Ga_2O_3	0.04	435	41	0.02
Unintentionally doped Ga_2O_3	0.09	195	28	0.08

(black and violet curve respectively) discussed in our previous work (line profiles extracted from figures 4(d) and 7(d) of [17]). As also reported in table 2, for these two samples it was not possible to determine their unintentional substrate offcut due to the fact that their crystals were already cut in small 5 × 5 mm^2 pieces. Nonetheless, it is interesting to notice that both (i) the presence of In during the deposition process (figure 4) and (ii) the presence of different unintentional substrate offcuts do not result in a significantly different mean facet length (table 2). In particular, the mean (110) facet length (equal to 1/2 of the peak-to-peak distance, i.e. ascending + descending (110)–$(\bar{1}10)$ facets, see figure 1(b)) is found to be around 5 nm. The validity of the extracted numbers from the AFM line profiles is ensured by the facet-to-facet length of ≈ 5 nm independently obtained from TEM cross sectional imaging of the MEXCAT sample reported in figure 8 of [17].

Next, in order to discuss the trenches, we report in figure 5 exemplary line profiles this time extracted along the [001] direction from the reported 5 × 5 μm^2 AFM images of figure 3 (color code of figure 5 in accordance to figure 3). In the case of the layers deposited on the two substrates having similar absolute offcuts (0.12° and 0.13°) with in-plane orientation 86° and 55° from the [001] direction, despite a low mean roughness of about 0.5 nm (figures 3 (a) and (b)), they both show similar trench-to-trench mean distance (≈ 450 nm) and trenches mean height of about 1–2 nm as indicated by the yellow and brown lines in figure 5 (note that the trench depth extracted from our AFM images is a lower bound estimate as it may be limited by the tip radius). Differently, the layer deposited on the substrate having lower in-plane offcut orientation (41°) from the [001] and the lowest absolute value (0.04°) results in a significantly rougher layer (rms ≈ 1.5 nm, figure 3(c)). This is related to the formation of deeper trenches (≈ 4–6 nm, red line in figure 5); nonetheless, we notice that the trench-to-trench mean distance is also significantly increased from the ≈ 450 nm of previous samples, to about 750 nm. Notably, the layer deposited on top of the substrate having the closest absolute offcut to the [001] in-plane direction (28°, absolute offcut value 0.09° figure 2 and figure 3(d)) is showing a trench-free morphology (blue line in figure 5).

In order to confirm our results, we performed a twin deposition (same growth conditions) on top of a second 5 × 5 mm^2 unintentionally doped substrate coming from the same 15 × 10 mm^2 crystal (reference deposition figure 3(d) and blue line in figure 5). The AFM pictures of the deposited layer (figure 6(a)) confirm the presence of a layer without the presence of trenches, whose rms is slightly lower than that of its twin deposited sample (rms ≈ 0.15 nm) and is just ruled by the (110)-faceting. Remarkably, it is possible to identify in this case the presence of monolayer steps whose direction and

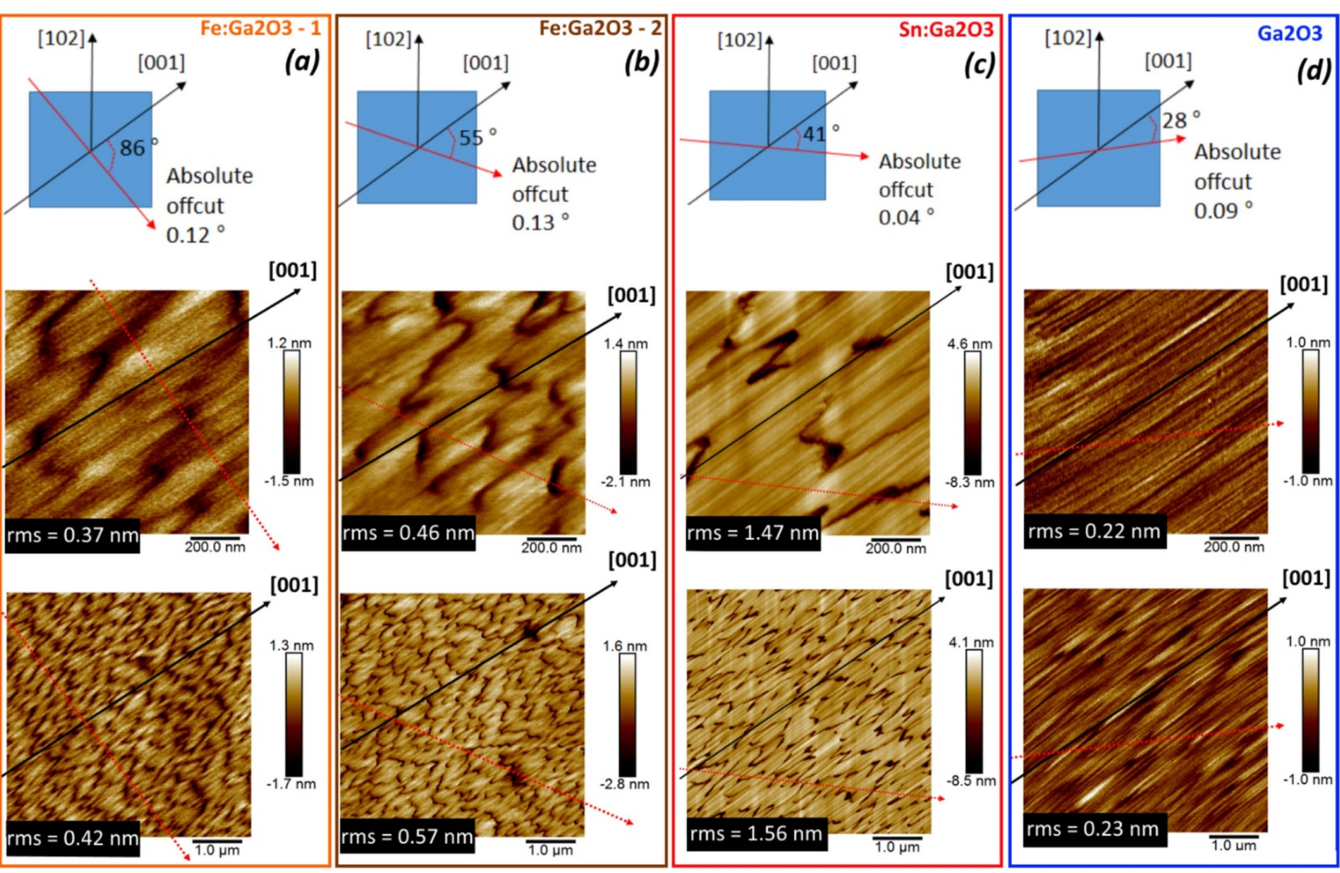

Figure 3. 1×1–5×5 μm^2 AFM images of (010) homoepitaxial layers grown under identical conditions by MEXCAT-MBE on four different substrates (a)–(d). The in-plane orientations are marked as black arrows while the measured absolute offcut directions and the absolute angles as red arrows in both a representative sketch of the substrates (top view) and the respective acquired AFM images of the layers deposited on top of them. Note that the bright vertical bands/lines in (c) are artifacts due to the vertical line-by-line flattening and the vertical scan direction.

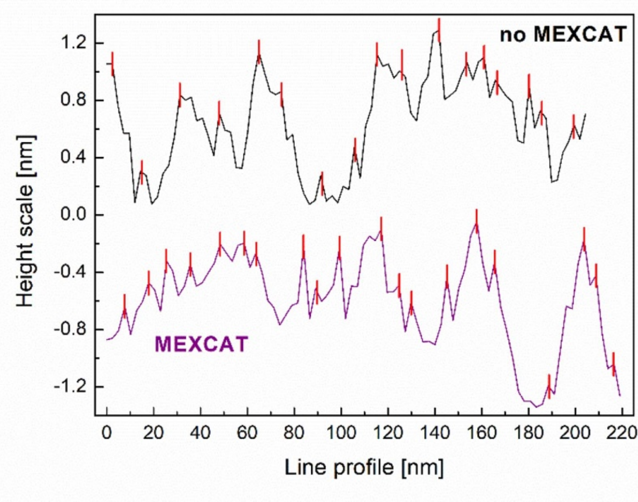

Figure 4. Line profiles extracted orthogonally to the [001] direction from the 1×1 μm^2 AFM images reported in figures 4(d) and 7(d) of [17] referring to homoepitaxial (010)-oriented layers deposited under the very same growth conditions with (violet curve) and without (black curve) MEXCAT; the identified peaks are marked in red.

Table 2. Mean peak-to-peak facet distance obtained from line profiles extracted orthogonal to the [001] in-plane direction (see figure 1) from AFM images presented in figure 3 and AFM images (1×1 μm^2) reported in figures 4(d) and 7(d) of [17]. An exemplary procedure to obtain this value is reported in figure 4 for these last two [17] samples.

Sample	Absolute offcut α (°)	Peak-to-peak facet mean distance (nm)
No MEXCAT [17]	Undetermined	**12**
MEXCAT [17]	Undetermined	**11**
Fe:Ga_2O_3–1	0.12	**9**
Fe:Ga_2O_3–2	0.13	**9**
Sn:Ga_2O_3	0.04	**13**
Ga_2O_3	0.09	**10**

spacing (figures 6(a) and (b) respectively) is in line with the measured substrate offcut (table 1 and figure 2). This evidence points towards a potential step-flow growth of the deposited (010) homoepitaxial layer.

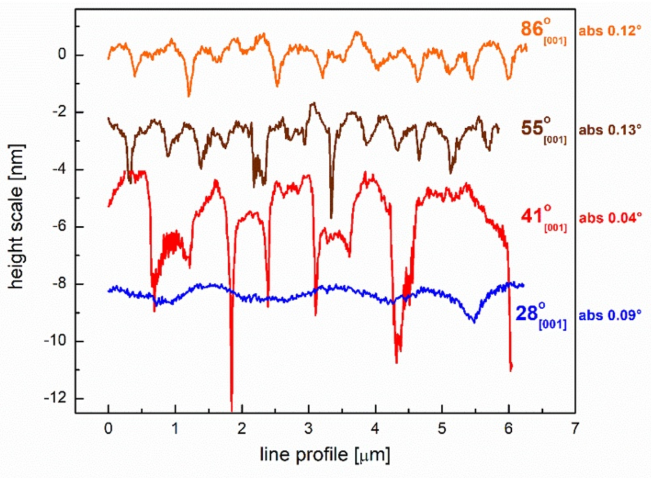

Figure 5. Line profiles extracted along the [001] direction from the $5 \times 5\ \mu m^2$ AFM images reported in figure 3 (line color code).

Finally, we investigated the effect of different Ga-to-O fluxes. We deposited on top of two $5 \times 5\ mm^2$ Sn:Ga_2O_3 substrates from the same investigated $15 \times 10\ mm^2$ crystal (table 1) at slightly higher (0.5 sccm) and lower (0.2 sccm) O-flows (reference O-flow = 0.33 sccm, figure 3(c)) while maintaining the same O-plasma P, T_g, and In-flux during the MEXCAT growth. A 0.2 sccm O-flow results in a surface morphology dominated by rougher (110)-facets with respect to the 0.33 sccm layer (figures 7(a) and 3(c) respectively). From figure 7(a) the presence of trenches is not clearly evident as in the case of the 0.33 sccm layer (figure 3(c)); the extracted line profiles along the [001] direction of the 0.2 sccm layer show the presence of smoother valleys with respect to the trenches evidenced in the sample deposited at 0.33 sccm (black and red lines respectively in figure 7(c)), but similar valley-to-valley periodicity (i.e. ≈ 750 nm). The XRD of the sample deposited at 0.2 sccm indicated neither In-incorporation nor thickness fringes (black curve in figure 7(d)), but it is reasonable to expect a thinner layer with respect to the 0.33 sccm layer (≈ 80 nm from XRD, see thickness fringes in red curve of figure 7(d)) due to the lower O-flow [16].

The slightly higher O-flow of 0.5 sccm resulted in the formation of clear trenches (figure 7(b)) whose mean trench-to-trench distance is strongly reduced with respect to the 0.33 sccm sample (≈ 200 nm versus ≈ 750 nm, green and red line respectively in figure 7(c)). Moreover, the O-richer deposition conditions resulted in (i) the presence of less defined (110)-facets (figure 7(b)) and (ii) the incorporation of a detectable amount of In ((020) left side shift, green line in figure 7(d)). This is expected given (i) the stability of the (010) surface under oxygen richer atmospheres [17] and (ii) the tendency to incorporate In in MEXCAT-MBE at high O-fluxes [5]. In this case, even though no fringes were detected (green line in figure 7(d)), we can safely assume that the thickness of the layer deposited at 0.5 sccm cannot significantly differ from the one of the samples deposited at 0.33 sccm (80–100 nm); in fact, it is known that higher O-fluxes result in higher metal incorporation [16], but in this case the Φ_{Ga} is already at its almost-upper limit (maximum layer thickness for the provided flux ≈ 100 nm) and it can be therefore exceeded just by the partial In-flux incorporation.

4. Discussion

It is reasonable to assume that the strong asymmetry of the monoclinic structure of β-Ga_2O_3 gives rise to anisotropic surface diffusion. Thus, we interpret the collected experimental results by anisotropic diffusion lengths and associated nucleation densities of the adsorbed species on the (010) Ga_2O_3 surface. While the presence of facets is related to the anisotropic surface free energy of β-Ga_2O_3 [17, 28], their width and the trench-to-trench distance can give quantitative evidence of the surface diffusion parallel and perpendicular to the [001] in-plane direction.

We consider first the morphology of a film shown in figure 4(d) of [17], that was grown without MEXCAT but at otherwise identical conditions (slightly metal-rich, i.e. 0.33 sccm) to those discussed in this work. In particular, we can consider the case of (i) the (110)-facets and (ii) the trenches. The (i) facets lateral size of this sample [17] of about 5 nm (the related AFM line profile is reported in figure 4 of the present work) is a good indication of the typical diffusion length of the adsorbed species orthogonal to the [001] direction. On the other hand, the (ii) large mean distance of about 300–500 nm [17] between trenches is suggesting a much larger diffusion length and associated lower nucleation density along the [001] direction. The experimental data of the present work for films grown under the same metal-to-oxygen flux ratio and substrate temperature but with In-mediated MEXCAT does not change this facet-and-trench morphology with respect to non-catalyzed MBE growth (compare figure 3 of the present work to figure 4(d) of [17]). An exemplary proof of this is the unchanged facet width of samples deposited with and without MEXCAT under the same growth conditions (figure 4 and table 2). Therefore, differently from what has been proposed elsewhere [24, 25], these experimental data suggest that In does not act as a surfactant, but just as a catalyst for the Ga_2O_3 layer growth.

Instead, our present work indicates that a sufficiently large absolute offcut mostly oriented along the [001] direction (unintentionally doped Ga_2O_3 substrate, see table 1 and figure 2) is the key for the formation of a trench-free (010) homoepitaxial layer (figures 3(d) and 6). The related monolayer steps (highlighted in figure 6) with spacing below or equal the diffusion length along the [001] direction of the surface-diffusing species can act as a regular array of nucleation sites. As shown by the presence of off-cut-related monolayer steps on the deposited layer shown in figure 6, this approach can eventually allow for step-flow growth in (010) homoepitaxy. Therefore, the resulting layers are homogeneously smooth with a low surface roughness (rms ≈ 0.2 nm) just ruled by the formation of the (110)-facets. The obtainment of such a low surface roughness despite the faceting is allowed by the low angle of the (110)-facets with respect to the (010) surface (≈ 14°, see figure 1(b)) and their limited lateral size (≈ 5 nm, see figure 4). We propose that the employment of proper offcuts could

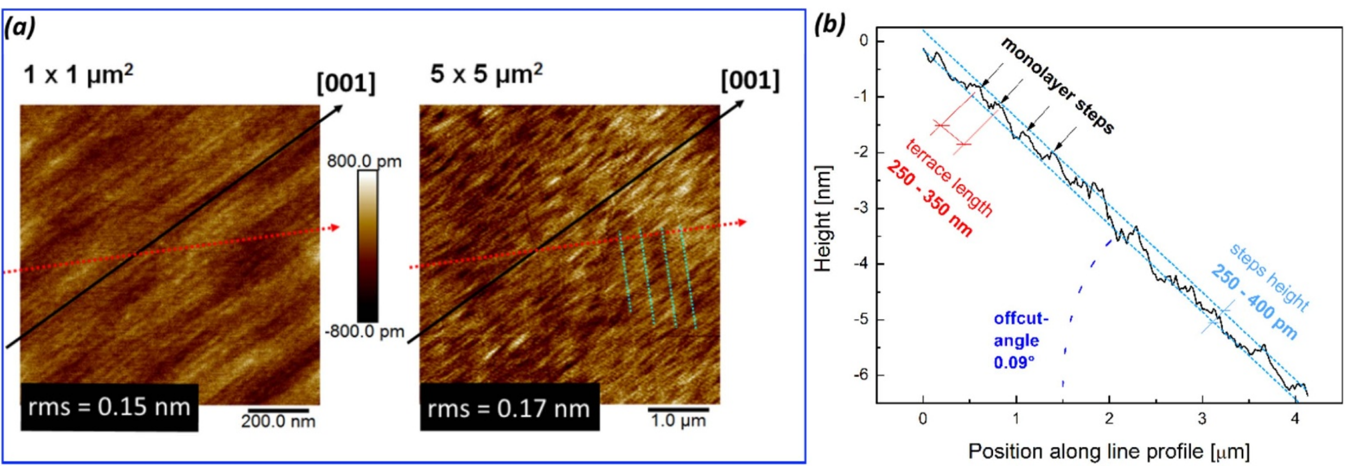

Figure 6. (a) AFM micrographs of a twin homoepitaxial deposition on top of a second 5 × 5 mm^2 piece of the unintentionally doped crystal (see figure 3(d)); the absolute offcut direction of the substrate is marked as a red arrow (details in table 1), while the presence of monolayer steps is evidenced by dotted cyan lines on the 5 × 5 μm^2 image. These monolayer steps are no artifacts as they are not aligned with the horizontal scan- and flattening-direction but are perpendicular to the offcut direction. (b) Line profile extracted from the 5 × 5 μm^2 AFM image along the offcut direction. A line was added to the profile to correctly reflect the offcut angle.

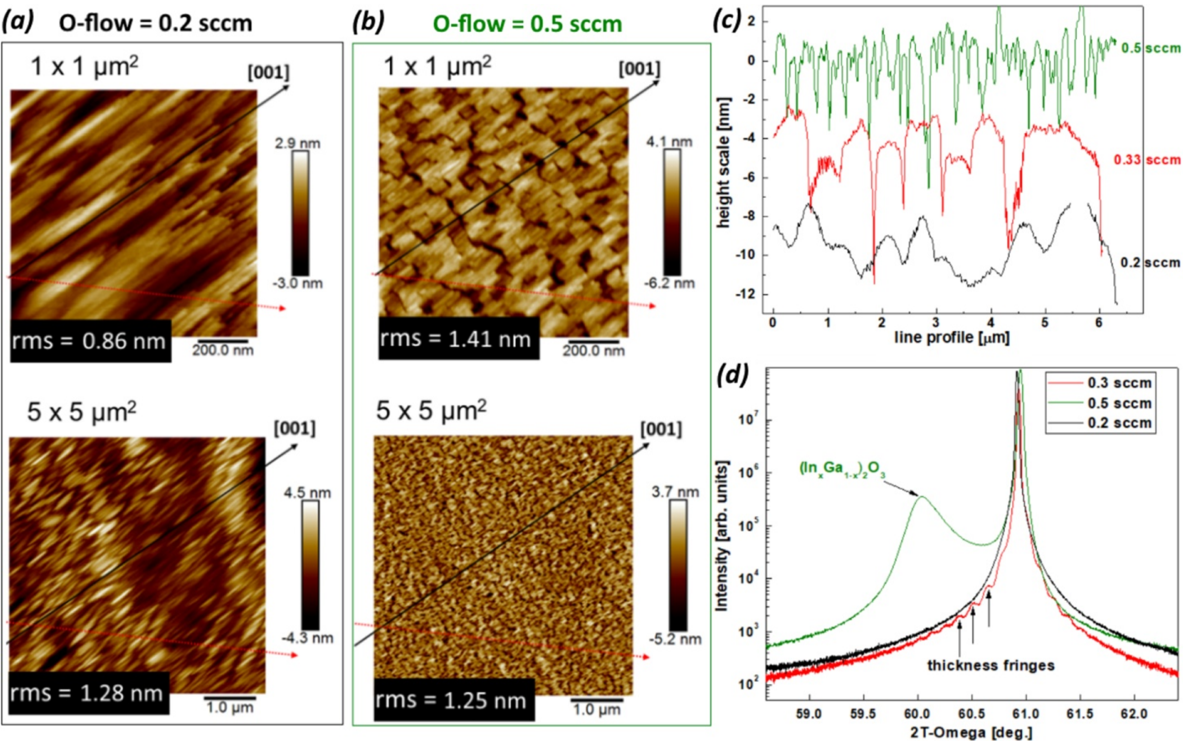

Figure 7. (a), (b) AFM micrographs of a homoepitaxial depositions on top of Sn-doped substrate at respectively lower (0.2 sccm) and higher (0.5 sccm) O-flow with respect to the reference layer (0.33 sccm, figure 3(c)). (c) Line profiles extracted along the [001] direction from the respective 5 × 5 μm^2 AFM images. (d) XRD of the reference layer (red curve) and the ones deposited at O-flows of 0.2 and 0.5 sccm (black and green curves respectively).

be fundamental for the growth of the highest surface quality β-Ga_2O_3 homoepitaxial layers on all the available substrate orientations since a well-defined substrate offcut has already allowed to achieve step flow growth in (100) β-Ga_2O_3 homoepitaxy by MOVPE [29].

Moreover, our data suggest that a too-low offcut and related long distance of monolayer steps (above the surface diffusion length) in the [001]-direction results in the random nucleation of islands whose coalescence forms the trenches during (010) homoepitaxy by plasma-assisted MBE with or without MEXCAT. An exception to this tentative explanation is the film grown on the substrate Fe:Ga_2O_3–2 which exhibits trenches (shown in figure 3(c)) despite an offcut component along the [001] (table 1) that is comparable to that of the trench-free film

grown on the unintentionally doped Ga_2O_3 substrate. Notwithstanding, this discrepancy suggests the actual absolute offcut direction along [001] to play a key role for obtaining trench-free layers.

In addition, the comparison among layers deposited on the same crystal with different O-to-Ga flux ratios allows us to identify the O-flow as an important parameter to change the diffusion length of the adsorbed species on the layer surface. In particular, while maintaining the same metal flux, a larger O-flow decreases the diffusion length (and increases the nucleation density) along the [001] direction resulting in the formation of closer spaced trenches (figures 7(b) and (c)).

We conclude that step bunching is not responsible for the formation of trenches that roughen the (010) layers in plasma assisted MBE since this mechanism—contrary to our observations—should be (i) promoted by the presence of a shorter distance of monolayer steps along the (high diffusion length) [001] direction rather than a longer one, and (ii) suppressed/reduced by a shorter diffusion length due to higher O-fluxes (0.5 sccm instead of 0.33 sccm) [30].

5. Conclusion

In conclusion, we found (010) β-Ga_2O_3 films homoepitaxially grown under slightly metal-rich conditions by plasma-assisted MBE with and without In-mediated MEXCAT to be significantly roughened due to the formation of trenches whereas the faceting into shallow (110)-$(\bar{1}10)$ facets elongated along the [001] direction plays a minor role for the total film roughness. The trench formation is likely related to coalescence boundaries due to an island growth regime with significantly higher diffusion length, and thus lower nucleation density, along the [001] direction than perpendicular to it. In agreement with this, the metal-to-oxygen flux ratio was identified as an important synthesis parameter that controls the diffusion length of the adsorbed species during layer growth and thus the trench density: a higher oxygen flux results in lower diffusion length and thus a higher density of trenches.

Using In-mediated MEXCAT, we demonstrate, that a sufficiently large substrate offcut oriented along the [001] direction can enable the growth of smooth, trench-free layers, i.e. about 100 nm thick with rms roughness as low as 0.2 nm, in (010) β-Ga_2O_3 homoepitaxy by plasma-assisted MBE. The absence of the trenches is tentatively attributed to the formation of proper monolayer steps whose width is comparable to or lower than the diffusion length of the surface diffusing species in that particular in-plane direction, indicating the possibility of step flow growth. The observed dependency of trench formation on offcut and oxygen flux excludes both (i) step bunching as their creation mechanism, as well as (ii) the possible role of In as a surfactant in (010) β-Ga_2O_3 homoepitaxy. We believe that this work can be fundamental for the realization of high quality interfaces and surfaces in multilayer heterostructures like β-$(Al_xGa_{1-x})_2O_3/Ga_2O_3$ on (010) β-Ga_2O_3 substrates with increased electron mobility due to reduced surface or interface roughness scattering.

Acknowledgments

We would like to thank Martin Albrecht, Konstantin Lion, and Stefano Cecchi for fruitful scientific discussion, Martin Heilmann for critically reading the manuscript, as well as Claudia Herrmann, Katrin Morgenroth, Hans-Peter Schönherr, and Carsten Stemmler for technical support. This work was performed in the framework of GraFOx, a Leibniz-ScienceCampus partially funded by the Leibniz association.

ORCID iDs

P Mazzolini https://orcid.org/0000-0003-2092-5265
O Bierwagen https://orcid.org/0000-0002-4746-5660

References

[1] Ahman J, Svensson G and Albertsson J 1996 *Acta Crystallogr., Sect.* C **52** 1336
[2] Higashiwaki M, Sasaki K, Kuramata A, Masui T and Yamakoshi S 2012 *Appl. Phys. Lett.* **100** 013504
[3] Baldini M, Galazka Z and Wagner G 2018 *Mater. Sci. Semicond. Process.* **78** 132
[4] Wagner G, Baldini M, Gogova D, Schmidbauer M, Schewski R, Albrecht M, Galazka Z, Klimm D and Fornari R 2014 *Phys. Status Solidi* a **211** 27
[5] Mazzolini P, Falkenstein A, Wouters C, Schewski R, Markurt T, Galazka Z, Martin M, Albrecht M and Bierwagen O 2020 *APL Mater.* **8** 011107
[6] Sasaki K, Kuramata A, Masui T, Víllora E G, Shimamura K and Yamakoshi S 2012 *Appl. Phys. Express* **5** 035502
[7] Okumura H, Kita M, Sasaki K, Kuramata A, Higashiwaki M and Speck J S 2014 *Appl. Phys. Express* **7** 095501
[8] Sasaki K, Higashiwaki M, Kuramata A, Masui T and Yamakoshi S 2014 *J. Cryst. Growth* **392** 30
[9] Baldini M, Albrecht M, Fiedler A, Irmscher K, Schewski R and Wagner G 2017 *ECS J. Solid State Sci. Technol.* **6** Q3040
[10] Zhang Y *et al* 2018 *Appl. Phys. Lett.* **112** 173502
[11] Ahmadi E, Koksaldi O S, Zheng X, Mates T, Oshima Y, Mishra U K and Speck J S 2017 *Appl. Phys. Express* **10** 071101
[12] Ranga P, Bhattacharyya A, Rishinaramangalam A, Ooi Y K, Scarpulla M A, Feezell D F and Krishnamoorthy S 2020 *Appl. Phys. Express* **13** 045501
[13] Zacherle T, Schmidt P C and Martin M 2013 *Phys. Rev.* B **87** 235206
[14] Kang Y, Krishnaswamy K, Peelaers H and de Walle C G V 2017 *J. Phys.: Condens. Matter* **29** 234001
[15] Lany S 2018 *APL Mater.* **6** 046103
[16] Vogt P and Bierwagen O 2018 *Phys. Rev. Mater.* **2** 120401
[17] Mazzolini P, Vogt P, Schewski R, Wouters C, Albrecht M and Bierwagen O 2018 *APL Mater.* **7** 022511
[18] Vogt P, Brandt O, Riechert H, Lähnemann J and Bierwagen O 2017 *Phys. Rev. Lett.* **119** 196001
[19] Kracht M *et al* 2017 *Phys. Rev. Appl.* **8** 054002
[20] Zhang Y, Joishi C, Xia Z, Brenner M, Lodha S and Rajan S 2018 *Appl. Phys. Lett.* **112** 233503
[21] Kaun S W, Wu F and Speck J S 2015 *J. Vac. Sci. Technol.* A **33** 041508
[22] Feng Z, Anhar Uddin Bhuiyan A F M, Karim M R and Zhao H 2019 *Appl. Phys. Lett.* **114** 250601
[23] Alema F, Zhang Y, Osinsky A, Valente N, Mauze A, Itoh T and Speck J S 2019 *APL Mater.* **7** 121110

[24] Vogt P, Mauze A, Wu F, Bonef B and Speck J S 2018 *Appl. Phys. Express* **11** 115503
[25] Baldini M, Albrecht M, Gogova D, Schewski R and Wagner G 2015 *Semicond. Sci. Technol.* **30** 024013
[26] Kuramata A, Koshi K, Watanabe S, Yamaoka Y, Masui T and Yamakoshi S 2016 *Japan. J. Appl. Phys.* **55** 1202A2
[27] Geller S 1960 *J. Chem. Phys.* **33** 676
[28] Schewski R *et al* 2018 *APL Mater.* **7** 022515
[29] Schewski R *et al* 2016 *J. Appl. Phys.* **120** 225308
[30] Burton W K, Cabrera N and Frank F C 1951 *Phil. Trans. Roy. Soc. London* **243** 299